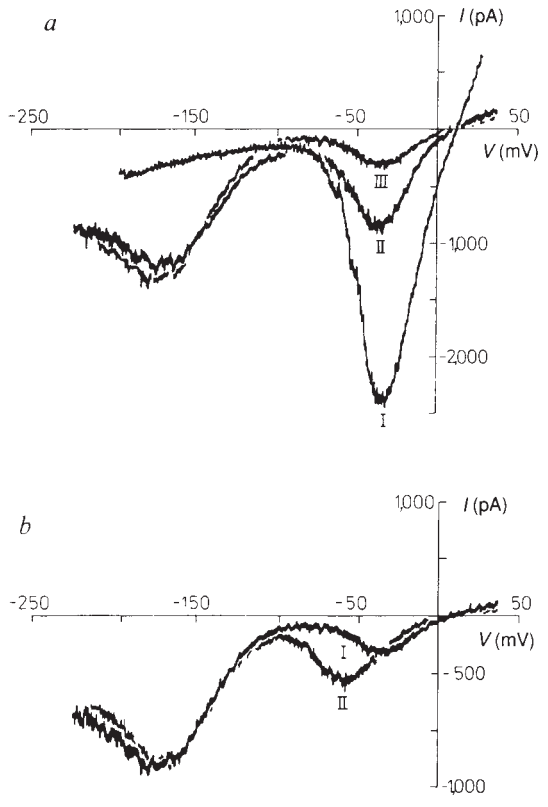

FIG. 5 Insensitivity of inward K^+ channels to auxins. *a*, Replacement of extracellular Ca^{2+} by K^+ causes a decrease in the anion current and an increase of the inward K^+ current. *b*, Simultaneous recording of voltage-dependent potassium and anion channels in the absence (AI and BI) and presence (BII) of 100 μM IAA. Current–voltage relations of K^+ and anion channels resulted from 1-s voltage ramps from a holding potential of −200 mV (AI) or −120 mV (AII, III and B). Note that potassium currents were not affected by auxin. Bath solutions in *a* were 40 mM $CaCl_2$, 2 mM $MgCl_2$, 10 mM MES/Tris, pH 5.6, and in *b*, 30 mM KCl, 2 $MgCl_2$, 2 mM $CaCl_2$, 10 mM MES/Tris, pH 5.6. Pipette solutions were identical to those mentioned in the legend to Fig. 2.

salts[15,16]. Evidence is accumulating that the (H^+)ATPase is activated by auxins through a complex signalling pathway which is supposed to include several receptor sites and coupling proteins[17], but to our knowledge this is the first evidence for a plant ion channel directly gated by extracellular growth hormones. □

Received 17 July; accepted 28 August 1991.

1. Raschke, K. *Encyclopedia of Plant Physiology* Vol. 7 383–441 (Springer, Berlin, 1979).
2. MacRobbie, E. A. C. *Bot. Acta* **101,** 140–148 (1988).
3. Snaith, P. J. & Mansfield, T. A. *J. exp. Botany* **33,** 360–365 (1982).
4. Keller, B. U., Hedrich, R. & Raschke, K. *Nature* **341,** 450–452 (1989).
5. Hedrich, R., Busch, H. & Raschke, K. *EMBO J.* **9,** 3889–3892 (1990).
6. Bates, G. W. & Goldsmith, M. H. *Planta* **159,** 231–237 (1983).
7. Felle, H., Peters, W. & Palme, K. *Biochim. biophys. Acta* (in the press).
8. Hamill, O. P., Marty, A., Neher, E., Sakmann, B. & Sigworth, F. J. *Pflügers Arch. ges. Physiol.* **391,** 85–100 (1981).
9. Schroeder, J. I., Hedrich, R. & Fernandez, J. M. *Nature* **312,** 361–362 (1984).
10. Rubery, P. H. & Sheldrake, A. R. *Planta* **118,** 101–121 (1974).
11. Hille, B. *Ionic Channels* (Sinauer, Sunderland, Massachusetts, 1983).
12. Schroeder, J. I., Raschke, K. & Neher, E. *Proc. natn. Acad. Sci. U.S.A.* **84,** 4108–4112 (1987).
13. Blatt, M. R. *J. Membr. Biol.* (in the press).
14. Busch, H., Hedrich, R. & Raschke, K. *Plant Physiol.* **93,** 17 (1990).
15. Hedrich, R. & Schroeder, J. I. *A. Rev. Plant Physiol.* **40,** 539–569 (1989).
16. Schroeder, J. I. & Hedrich, R. *Trends Biochem. Sci.* **5,** 187–192 (1989).
17. Palme, K. *Int. Rev. Cytol.* **132,** 223–283 (1992).

ACKNOWLEDGEMENTS. This work is dedicated to J. I. Schroeder and M. Spors (9 August 1991). We thank H. Depta (Göttingen) for discussion, R. Hertel (Freiburg), E. Neher (Göttingen) and D. G. Robinson (Göttingen) for comments on the manuscript, and K. Raschke and D. G. Robinson for laboratory facilities. This work was supported by grants from DFG to R.H.

Structure of domain 1 of rat T lymphocyte CD2 antigen

Paul C. Driscoll*, Jason G. Cyster†, Iain D. Campbell*, & Alan F. Williams†

* Department of Biochemistry, University of Oxford, Oxford OX1 3QU, UK
† MRC Cellular Immunology Research Unit, Sir William Dunn School of Pathology, University of Oxford, Oxford OX1 3RE, UK

THE CD2 antigen is largely restricted to cells of the T-lymphocyte lineage and has been established as an important adhesion molecule in interactions between human T lymphocytes and accessory cells[1]. In the adhesion reaction, CD2 on T cells binds to LFA-3 on other cells, with binding through domain 1 of CD2 (ref. 2). CD2 can also be a target for the delivery of mitogenic signals to T lymphocytes cultured with combinations of anti-CD2 antibodies[3,4]. Two predictions that are contradictory have been made for the structure of CD2 domain 1. One suggests an immunoglobulin (Ig) fold, on the basis of sequence patterns conserved in the Ig-superfamily (IgSF)[5], whilst the other proposes a pattern of alternating α-helices and β-strands, on the basis of

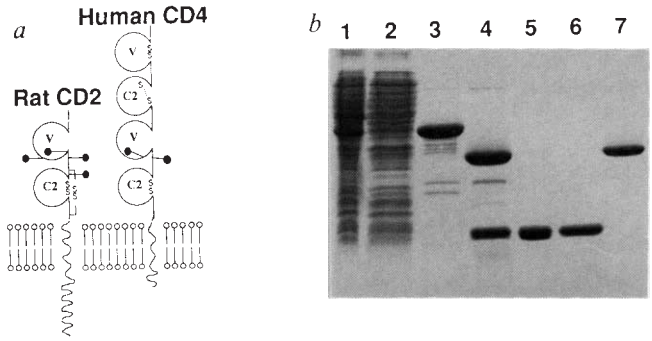

FIG. 1 *a*, Schematic representations for CD2 and CD4 at a cell surface. The circles indicate IgSF domains and the ♀ symbols, N-linked carbohydrate structures. *b*, Expression and purification of rat CD2 domain 1. Lanes: 1, soluble lysate from *E. coli* expressing the fusion protein of GST–CD2 domain 1; 2, lysate passed through a glutathione agarose affinity column; 3, purified fusion protein; 4, fusion protein cleaved with thrombin; 5 and 6, CD2 domain 1 after purification by affinity chromatography followed by gel filtration; 7, GST.

METHODS. Nucleotide sequence encoding rat CD2 protein residues 1–99 was isolated from the complementary DNA[7] by polymerase chain reaction (PCR) with the introduction of a *Bam*H1 restriction site immediately preceding the codon for protein residue 1 and a stop codon after the codon for amino-acid 99 followed by an *Eco*R1 site. The PCR product was inserted into the pGEX-2T vector and the sequence was confirmed using oligonucleotides specific for pGEX. The construct was transformed into *E. coli* BL21, a prototrophic strain. For fusion protein production, cells were grown overnight, diluted 1:10 in fresh medium and grown for 1 h at which point IPTG (isopropylthiogalactoside) was added to 0.12 mM, and the cells grown for a further 3 h. The cells were pelleted and resuspended in 1/60 volume 25 mM Tris–HCl, pH7.4, 150 mM NaCl, 5 mM EDTA, 0.2 mM PMSF, 2 mM iodoacetamide acid and sonicated for 3 × 30 s using an MSE sonicator on amplitude setting 8. Triton X-100 was added to a final concentration of 1% and the lysate spun at 30,000*g* for 30 min. The supernatant was passed over a glutathione-agarose column which was then washed with 25 mM Tris–HCl pH7.4, 140 mM NaCl and eluted with 5 mM glutathione, 50 mM Tris–HCl, pH8. The eluted material was mixed with 0.05 vol 3 M NaCl, 50 mM $CaCl_2$ and 1 NIH u of bovine thrombin per 2 mg protein. Cleavage was complete after 60 min and the CD2 domain was then purified on an OX34 monoclonal antibody affinity column[7] followed by gel filtration using a 200 ml Sephadex G75 column. For ^{15}N-labelling, cells were grown in M9 medium (10 mM $MgSO_4$, 1 mM $CaCl_2$, 0.4% glucose, 48 mM Na_2HPO_4, 22 mM KH_2PO_4, 9 mM NaCl) and $^{15}NH_4Cl$ (MSD Isotopes, Merck Frost, Canada) at 9.7 mM for ~18 h until the absorbance at 550 nm (A_{550}) was >1.0. The cells were then diluted 1:10 and grown for 2 h until A_{550} = ~0.5 when IPTG was added and growth continued for a further 3–4 h.

secondary structure predictions[6]. Thus CD2 domain 1 is an important test case for the validity of IgSF assignments based on sequence patterns. We report here the expression of domain 1 of rat CD2 in an *Escherichia coli* expression system and have determined a low-resolution solution structure by NMR spectroscopy.

A schematic model proposed for the domain structure of CD2 is shown in Fig. 1*a* together with that for CD4 whose extracellular region may have been derived in evolution from a CD2-like structure by gene duplication of a two-domain segment[7,8]. Domain 1 of rat CD2 was considered to encompass amino-acid residues 1–99 and this sequence was expressed as a fusion protein with glutathione-S-transferase (GST) of the blood fluke *Schistosoma mansoni*[9] in *E. coli* with the thrombin cleavage sequence, LVPRGS, between GST and CD2 domain 1. Thrombin cleaves after the Arg(R) residue in this sequence and thus the cleaved product contains the extra residues Gly Ser at the amino terminus of the CD2 domain 1 sequence. The fusion protein was expressed at 40 mg l^{-1} and was soluble in the lysate of *E. coli* cells, allowing purification on a glutathione agarose column (Fig. 1*b*, lanes 1–3). Cleavage by thrombin was effective and the CD2 domain was purified by affinity chromatography followed by gel filtration (Fig. 1*b*, lanes 4, 5 and 6). The CD2 domain was judged to be folded correctly because it bound to two noncompetitive monoclonal antibodies against rat CD2 (OX34 and OX55) (ref. 4) with an affinity equal to that of the extracellular domain of CD2 expressed in Chinese hamster ovary cells (data not shown). The fusion protein was also expressed in *E. coli* cells grown with $^{15}NH_4Cl$ as the sole nitrogen source to yield uniformly ^{15}N-labelled CD2 domain 1, suitable for multidimensional heteronuclear (NMR) studies.

The CD2 domain 1 preparations yielded excellent NMR spectra and the assignment of the ^1H resonances to individual amino acids was done using a combination of three-dimensional ^1H nuclear Overhauser enhancement ^{15}N-^1H heteronuclear multiple quantum coherence (NOESY-HMQC) and ^1H homonuclear Hartmann-Hahn-^{15}N-^1H-HMQC (HOHAHA-HMQC) NMR spectroscopy[10,11]. Side-chain assignments were obtained using two-dimensional ^1H NMR of an unlabelled sample of the protein in D_2O solution.

Three-dimensional structures for CD2 domain 1 were calculated on the basis of the NOE data, slowly exchanging amide NH groups and $^3J_{NH\alpha}$ spin-spin coupling constants. The

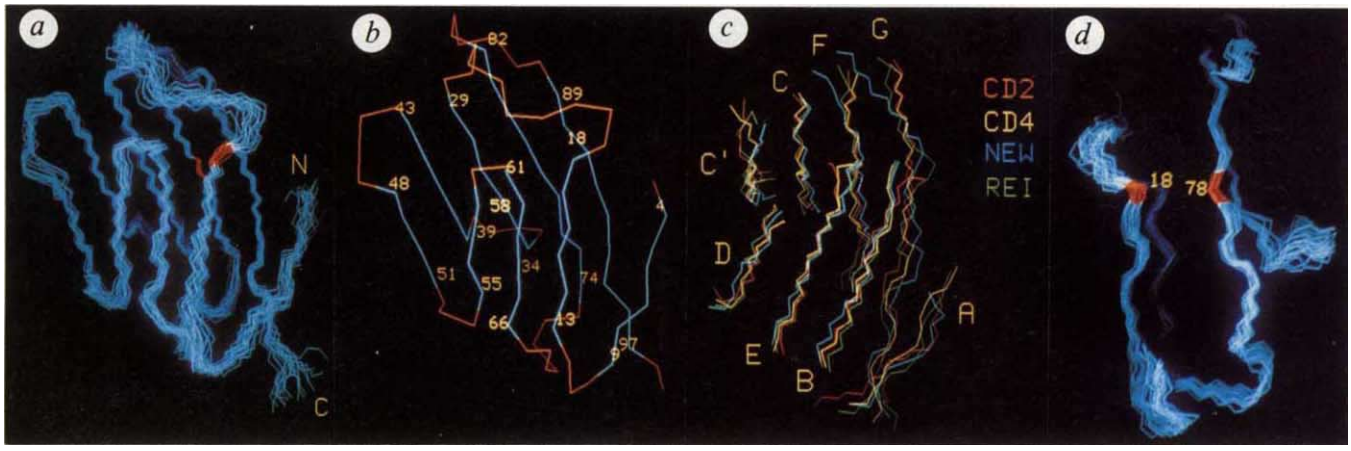

FIG. 2 *a*, Best-fit superposition of the 16 structures computed for CD2 domain 1 based on 713 NOE distance restraints (20 intraresidue, 346 sequential (residue *i*, residue *j*; $j=i+1$), 102 short range (i, j; $j \leq i+5$), 60 medium range (i, j; $j \leq i+10$) and 185 long range (i, j; $j > i+10$), 64 ϕ dihedral angle restraints and 68 H-bond distance restraints. Backbone N, C and Cα atoms of residues 5–98 are shown. NMR spectra were recorded using a 3 mM pH4.2 CD2 domain 1 sample, at 500 or 600 MHz ^1H frequency and at 23 °C or 30 °C. Distance restraint upper limits were categorized according to the estimated intensity of the NOE cross peak in the spectrum: strong 2.7 Å; medium 3.5 Å; weak 5.0 Å. Appropriate corrections were made to the upper limits in the cases of NOEs connecting degenerate proton resonances. Sequential distance restraints were estimated on a 10-point sliding scale from the integrated cross-peak intensities of the three-dimensional ^{15}N-^1H NOESY-HMQC NMR experiment (mixing time = 150 ms). In all cases the lower limit of the distance restraint was given by the van der Waals' contact distance. $^3J_{NH\alpha}$ spin-spin coupling constants were measured by lineshape fitting the traces from a two-dimensional ^{15}N-^1H HMQC-*J* experiment[27]. For $^3J_{NH\alpha}$ smaller than 6 Hz the corresponding ϕ torsion angle was restrained in the range −20° to −105°; for $^3J_{NH\alpha}$ larger than 7.5 Hz the ϕ angle was restrained to the range −70° to −120°. H-bonded amide NH groups were identified on the basis of the presence of an NH resonance 2 h after dissolving the protein in D_2O solution. The distance restraints used for each H-bond identified were r(HN-O) ≤ 2.3 Å, r(N-O) = 2.5–3.3 Å. Initially 30 structures were computed starting from randomized coil structures using a dynamical simulated annealing protocol[12,13] using the program X-PLOR. After two rounds of refinement in which the NOE restraints list was revised and added to, 16 structures had converged with good covalent geometry and van der Waals' contacts and no single violation greater than 0.5 Å. During the calculations the protein moves in a force field consisting of the sum of a number of terms. Bond (F_{bond}) and angle terms (F_{angle}) are used to maintain idealized covalent geometry. An improper dihedral term ($F_{improper}$) is incorporated to maintain the planarity and chirality of certain covalent groups including the peptide bond which is assumed to be planar and universally *trans* in CD2 domain 1. Square well terms are used for experimental distance (F_{NOE}) and dihedral angle restraints (F_{cdihed}). A simple quartic repulsion term (F_{vdW}) is used to represent the van der Waals' component of the target function. The N-terminal region of the protein, comprising the Gly-Ser N-leader dipeptide and residues 1 and 2, was omitted from the calculations because of the absence of structurally significant NMR data. The final values of each term of the target function for the 16 structures were: $F_{bond} = 72 \pm 4$ kcal mol^{-1}; $F_{angle} = 1842 \pm 14$ kcal mol^{-1}; $F_{improper} = 100 \pm 4$ kcal mol^{-1}; $F_{NOE} = 168 \pm 18$ kcal mol^{-1}; $F_{cdihed} = 4.5 \pm 2$ kcal mol^{-1}; $F_{vdW} = 59 \pm 8$ kcal mol^{-1}; $F_{total} = 2{,}247 \pm 38$ kcal mol^{-1}. For each of these terms the final force constant used was identical to that given in ref. 12. The hard sphere van der Waals' radii were set to 0.8 of the standard values. Using the CHARMM[28] empirical energy function to measure a Lennard-Jones van der Waals' energy for each structure gave a value $E_{L-J} = -243 \pm 12$ kcal mol^{-1}, indicating good nonbonded contacts. Note that this Lennard-Jones term is not used as part of the target function in the structure calculations. The rms deviations from the experimental restraints and idealized covalent geometry are small: interproton distances (781) 0.085 ± 0.004 Å; experimental dihedral constraints (64) 1.047 ± 0.266 degree; bonds (1552) 0.010 ± 0.0003 Å; angles (2979) 2.078 ± 0.008 degree; improper dihedrals (634) 1.023 ± 0.018 degree. *b*, The backbone Cα trace of the mean structure for CD2 domain 1 computed from the 16 best-fitted structures by coordinate averaging and energy minimization. The β strands are shown in blue, loops in red. *c*, The β sheets of CD2 superimposed with those of CD4 and REI V_L and NEW V_H. The structures were aligned with each other by matching 28 Cα positions of the core residues of β strands B, C, D, E and F. *d*, A cutaway view of the superimposed CD2 structures showing the Ile-18 and Val-78 residues (with Cα atoms coloured red) that are at the positions of the conserved IgSF disulphide bond in antibody V-domains. The separation of the Cα atoms of these residues is the range observed for disulphide links in IgSF domains.

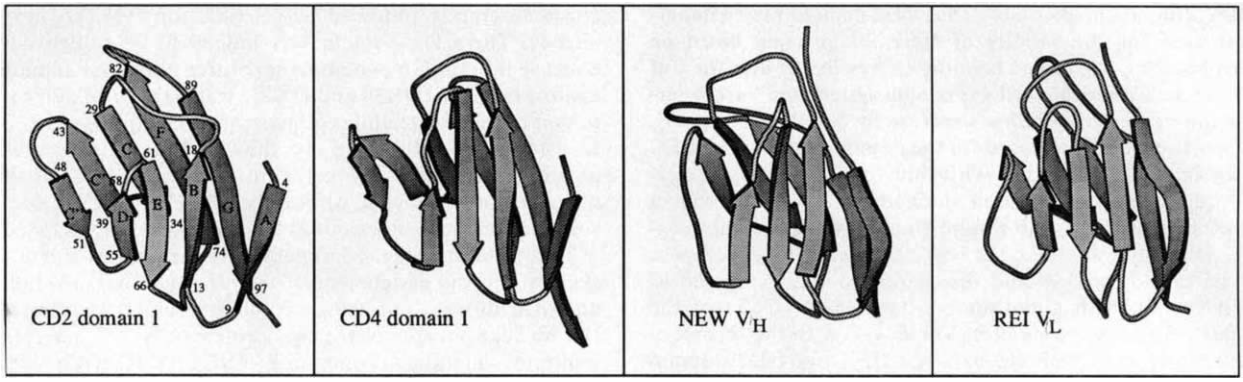

FIG. 3 Illustrations of the folds for CD2 domain 1, CD4 domain 1, immunoglobulin NEW V_H and immunoglobulin REI V_L. The coordinates for CD4 domain 1 were kindly provided by S. Harrison and those for the V domains were from the Brookhaven database. The diagrams were computed using the MOLSCRIPT program[29].

calculations were done using the X-PLOR program based on dynamical simulated annealing[12,13]. In total, 16 independent structures were obtained that satisfied the NOE distance restraints with no violation in any individual structure greater than 0.5 Å. The structures were based on 713 interproton NOE distance restraints, 64 ϕ dihedral angle restraints and 68 H-bond distance restraints. The 16 structures are shown in Fig. 2*a*, best-fitted on the backbone atoms of residues 3–98. A restrained minimized average structure was obtained by computing the mean coordinate positions of the 16 best-fitted structures followed by restrained minimization of the same target function as that used in the final stages of the structure calculation (Fig. 2*b*). The r.m.s. deviation of the 16 structures from the restrained minimized average structure is 0.98 ± 0.11 Å for backbone atoms and 1.59 ± 0.19 Å for all atoms in the well-defined portion of the structure spanning residues 3–98. This level of definition is sufficient to determine accurately the polypeptide fold of the protein and the conformation of some of the internal side chains.

The calculated CD2 structures clearly show a fold like an immunoglobulin V-domain and in Fig. 2*c* the β strands for CD2 are overlayed with equivalent strands from CD4 (refs 14, 15) and the immunoglobulin V domains NEW V_H (ref. 16) and REI V_L (ref. 17). It can be seen that the core strands are very similar with r.m.s. differences for the three-dimensional alignments being 0.92, 1.43 and 0.95 Å for CD2 versus CD4 and the V_H and V_L domains, respectively (calculations for 28 Cα positions from β strands B, C, D, E and F).

Ile 18 and Val 78 are the residues of CD2 domain 1 corresponding to the conserved disulphide bond of IgSF domains[5] and these residues are highlighted in Fig. 2*d*. In the 16 structures the Cα atoms of these residues are separated by 7.0 ± 0.2 Å. In IgSF domains the Cα–Cα distance of the Cys residues forming the conserved disulphide bond is in the range 5.6–7.4 Å (ref. 18). In studies before the determination of the CD2 stucture, cysteine residues were substituted by site-directed mutagenesis at Ile 18 and Val 78 and the mutant CD2 was expressed in a secreted two-domain form in Chinese hamster ovary cells. In this CD2 mutant a disulphide bond was formed (F. Gray, J.G.C., T. Willis, A.F.W. manuscript in preparation).

When the full CD2 domain is compared with CD4 domain 1 and the V-domains, differences in the regions connecting the β-strands are evident. Figure 3 shows comparisons of the folds for the four domains and the sequence comparisons for CD2 and CD4 are shown in Fig. 4. After the Ile-18 residue of β-strand

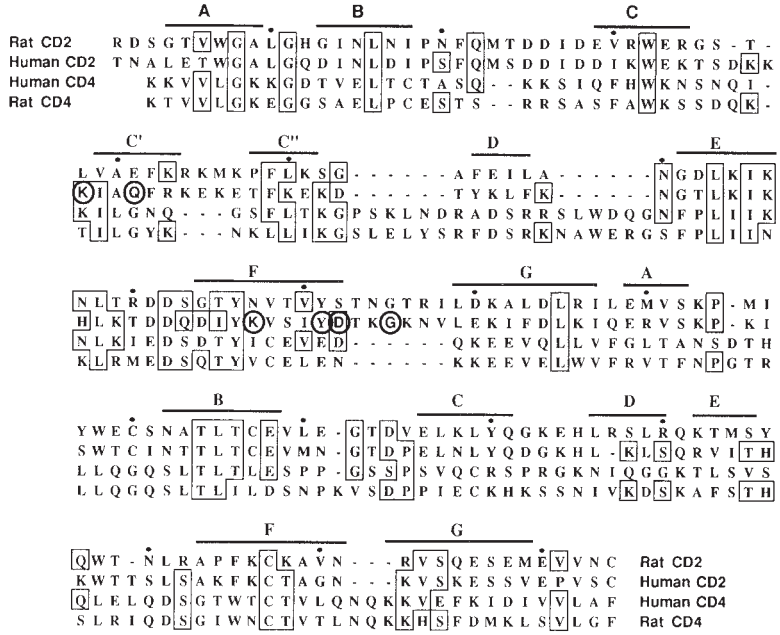

FIG. 4 Sequence alignments of CD2 and CD4 domains 1 and 2. Human and rat sequences are shown derived from the Swissprot database. The first three amino acids of human CD2 are not shown and the black dots above the rat CD2 sequence indicate each tenth residue of that sequence. The β-strand assignments have been made on the basis of the rat CD2 structure for the first domains and on the basis of the CD4 structure for the second domains. In the domain 1 sequences, the positions of CD4 β strands are also correctly identified by the bars but their extent is not exactly shown in all cases. Residues in human CD2 that are candidates for involvements in LFA-3 binding are circled and include human residues 43, 46, 82, 86, 87 and 90. These data are from mutational analysis[19] (note residue 43 is equivalent to 48 in ref. 19 where the amino terminus was assigned five residues before the correct position). The criteria for considering a residue as a candidate for binding is that there should be a single mutation, not involving a Pro residue, that leads to the loss of LFA-3 binding and that the equivalent residue in the rat structure (38, 41, 77, 81, 82 and 85) is accessible to solvent. All of these residues except rat Ser 82 are exposed on the same β-sheet face.

B in CD2, there is a Pro residue and the CD2 chain folds immediately into a long, kinked loop connecting to β-strand C. In the V domains and CD4, β-strand B extends further and the loop joining strands B and C is not distorted. In CD2, βstrands D and E are truncated in comparison with the same regions in the other domains. This seems to be required to accommodate the kink in the loop between strands B and C since there are many internal side-chain contacts between the loops connecting strands B to C and D to E. These contacts plus the unusual structure for the B to C loop may explain the fact that sequence in this region is highly conserved between human and rat CD2. By contrast, in the same region of CD4 there is little conservation of sequence between the species (Fig. 4). In CD2 the loop between β-strand F and G is longer than in CD4 and is more similar to the same region in the V-domains where this loop constitutes hypervariable region 3.

The structure for CD4 (refs 14, 15) is unusual in comparison with immunoglobulin chains in that domain 2 follows on directly from domain 1 without any hinge residues such as are found between immunoglobulin V domains and the following C_L or C_{H1} domains. From Fig. 4 it is probable that the juxtaposition of domains in CD2 will be like that in CD4 as the distance of the β-strand G of domain 1 from β-strand B of domain 2 is one amino acid less in the CD2 sequence than in CD4.

The β-strand assignments for human CD2 domain 1 can be made by alignment with the newly solved rat CD2 domain 1 structure (Fig. 4). All the LFA-3 binding activity resides in domain 1 of CD2 (ref. 2) and mutagenesis of human CD2 has indicated regions of contact with LFA-3 (ref. 19). Residues which appear to be involved in this interaction are marked in Fig. 4. These are positioned in β-strand C′ and in the region of β-strands F to G. This suggests that the face of the β-sheet C, C′, C″, F, G may be involved in the CD2:LFA-3 interaction. This can be further investigated by mutation analysis on the basis of the known three-dimensional structure.

The structure of CD2 domain 1 fits closely with that predicted from sequence on the basis of superfamily considerations with β-strands B, C, E and F that make up the core of the fold being exactly predicted[5,7]. The proposal from secondary structure predictions[2,6] is incorrect. CD2 domain 1 and CD4 domain 2 (refs 14, 15) were test cases for IgSF arguments because both sequences had unusual features which lead to contradictions between predictions from superfamily sequence patterns[8] and *ab initio* computer calculations based on the primary sequences. The superfamily arguments were correct in both cases and this suggests that other IgSF domains predicted on the basis of conserved sequence patterns will also be correct[20].

The structure for CD2 domain 1 adds significantly to known variants of the immunoglobulin-fold as it is the first structure for a domain involved in cell adhesion and provides a prototype for IgSF domains that lack the conserved disulphide bond. Structures determined previously include immunoglobulin V and C domains[21], MHC class 1 α3 domain[22] and β-2 microglobulin[22,23] and CD4 domains 1 and 2 (refs 14, 15). Also immunoglobulin-like folds have been seen in domains 1 and 2 of the PapD bacterial chaperone protein[24], but these should not be categorized as IgSF domains as they show no detectable sequence similarity to IgSF domains (ref. 25 and A.F.W., unpublished data). CD2 domain 1 typifies IgSF domains that lack the conserved disulphide bond. Such domains are found at a moderate frequency among domains of cell-surface molecules (for example LFA-3 domain 1, CEA domain 1, CD4 domain 3, PDGF receptor domain 4 (ref. 20)) but are the main type in the myosin-binding muscle proteins that are in the IgSF (ref. 26). □

Received 4 July; accepted 23 August 1991.

1. Springer, T. A. *Nature* **346,** 425–434 (1990).
2. Recny, M. A., Neidhardt, E. A., Sayre, P. H., Ciardelli, T. L. & Reinherz, E. L. *J. biol. Chem.* **265,** 8542–8549 (1990).
3. Meuer, S. C. *et al. Cell* **36,** 897–906 (1984).
4. Beyers, A. D., Barclay, A. N., Law, D. A., He, Q. & Williams, A. F. *Immun. Rev.* **111,** 59–77 (1989).
5. Killeen, N., Moessner, R., Arvieux, J., Willis, A. & Williams, A. F. *EMBO J.* **7,** 3087–3091 (1988).
6. Clayton, L. K., Sayre, P. H., Novotny, J. & Reinherz, E. L. *Eur. J. Immun.* **17,** 1367–1370 (1987).
7. Williams, A. F., Barclay, A. N., Clark, S. J., Paterson, D. J. & Willis, A. C., *J. exp. Med.* **165,** 368–380 (1987).
8. Williams, A. F.,Davis, S. J., He, Q. & Barclay, A. N. *Cold Spring Harb. Symp. quant. Biol.* **54,** 637–647 (1989).
9. Smith, D. B. & Johnson, K. S. *Gene* **67,** 31–40 (1988).
10. Marion, D. *et al. Biochemistry* **28,** 6150–6156 (1989).
11. Driscoll, P. C., Clore, M., Marion, D., Wingfield, P. T. & Gronenborn, A. M. *Biochemistry* **29,** 3542–3556 (1991).
12. Clore, G. M. & Gronenborn, A. M. *CRC crit. Rev. Biochem. molec. Biol.* **24,** 479–564 (1989).
13. Brünger, A. T. *X-PLOR Manual, Version 2.1* (Yale University Press, 1990).
14. Wang, J. *et al. Nature* **348,** 411–418 (1990).
15. Ryu, S-E. *et al. Nature* **348,** 419–426 (1990).
16. Saul, F. A., Amzel, M. & Poljak, R. J. *J. biol. Chem.* **253,** 585–597 (1978).
17. Epp, O., Lattman, E. E., Schiffer, M., Huber, R. & Palm, W. *Biochemistry* **14,** 4943–4952 (1975).
18. Richardson, J. S. *Adv. Protein Chem.* **34,** 167–339 (1981).
19. Peterson, A. & Seed, B. *Nature* **329,** 842–846 (1987).
20. Williams, A. F. & Barclay, A. N. *A. Rev. Immun.* **6,** 381–405 (1988).
21. Amzel, L. M. & Poljak, R. J. *A. Rev. Biochem.* **48,** 961–967 (1979).
22. Bjorkman, P. J. *et. al. Nature* **329,** 506–512 (1987).
23. Becker, J. W. & Reeke, G. N. *Proc. natn. Acad. Sci. U.S.A.* **82,** 4225–4229 (1985).
24. Holmgren, A. & Branden, C.-I. *Nature* **342,** 248–251 (1989).
25. Freeman, M. *et al. Proc. natn. Acad. Sci. U.S.A.* **87,** 8810–8814 (1990).
26. Labiet, S. *et al. Nature* **345,** 273–276 (1990).
27. Kay, L. E. & Bax, A. *J. Magn. Reson.* **86,** 110–126 (1990).
28. Brooks, B. R. *J. comput. Chem.* **4,** 187–217 (1983).
29. Kraulis, P. *J. J. appl. Crystallogr.* (in the press).

ACKNOWLEDGEMENTS. We thank J. Boyd, T. Harvey and N. Soffe from the Oxford Department of Biochemistry for helpful discussions and S. Harrison, Harvard University for supplying the CD4 coordinates. I.D.C. is a member of the Oxford Centre for Molecular Sciences supported by the SERC and MRC. P.C.D. is supported by a Royal Society University Research Fellowship and J.G.C. by a Commonwealth Overseas Studentship.

Elimination from peripheral lymphoid tissues of self-reactive B lymphocytes recognizing membrane-bound antigens

Suzanne B. Hartley*†, Jeffrey Crosbie*, Robert Brink*, Aaron B. Kantor‡, Antony Basten* & Christopher C. Goodnow†

* Centenary Institute of Cancer Medicine and Cell Biology, University of Sydney, New South Wales 2006, Australia
† Howard Hughes Medical Institute, and Department of Microbiology and Immunology, and ‡Department of Genetics, Beckman Center for Molecular and Genetic Medicine, Stanford University, Stanford, California 94305-5428, USA

THE long-standing hypothesis[1,2] that tolerance to self antigens is mediated by either elimination[3–8] or functional inactivation (anergy; refs 9–11) of self-reactive lymphocytes is now accepted, but little is known about the factors responsible for initiating one process rather than the other. In the B-cell lineage, tolerant self-reactive cells persist in the peripheral lymphoid organs of transgenic mice expressing lysozyme and anti-lysozyme immunoglobulin genes[9], but are eliminated in similar transgenic mice expressing anti-major histocompatibility complex immunoglobulin genes[8]. By modifying the structure of the lysozyme transgene and the isotype of the anti-lysozyme immunoglobulin genes, we demonstrate here that induction of anergy or deletion is not due to differences in antibody affinity or isotype, but to recognition of monomeric or oligomeric soluble antigen versus highly multivalent membrane-bound antigen. Our findings indicate that the degree of receptor crosslinking can have qualitatively distinct signalling consequences for lymphocyte development.

The soluble lysozyme gene construct used earlier[9] was modified to encode an integral membrane protein by inserting a complementary DNA fragment encoding the extracellular spacer sequence, transmembrane segment and cytoplasmic tail